Chemistry of the Galactic Bulge: New Results

Manuela Zoccali[1]
Vanessa Hill[2]
Beatriz Barbuy[3]
Aurelie Lecureur[4, 5]
Dante Minniti[1, 6]
Alvio Renzini[7]
Oscar Gonzalez[1]
Ana Gómez[2]
Sergio Ortolani[8]

[1] Departamento de Astronomía y Astrofísica, Pontificia Universidad Católica de Chile, Chile
[2] CNRS, Observatoire de la Côte d'Azur, France
[3] Universidade de São Paulo, Brazil
[4] GEPI, Observatoire de Paris, France
[5] Astronomisches Rechen-Institut, Zentrum für Astronomie der Universität Heidelberg, Germany
[6] Vatican Observatory, Italy
[7] INAF–Osservatorio Astronomico di Padova, Italy
[8] Università di Padova, Dipartimento di Astronomia, Italy

VLT–FLAMES observations provide by far the largest sample of high dispersion spectra of Bulge red giants available. Five years of work on these 900 spectra have yielded the abundances of different elements in the Milky Way Bulge, and new results on its formation. The results so far include the Bulge metallicity distribution, the Bulge metallicity gradient, the metallicity dependence on kinematics, the history of enrichment with alpha-elements, as well as the lithium abundance. The evidence collected on Milky Way Bulge chemical enrichment supports a rapid early formation scenario, and the metallicity gradient argues against formation via secular bar evolution.

Introduction to the Milky Way Bulge: a complex evolution?

The central part of our Milky Way galaxy is called the Bulge, and it is the region that contains the densest concentration of baryonic matter. We live in the Galactic disc, a relatively calm place in comparison with the Bulge, which might have had a very complex formation and evolution. Unravelling the whole history of the evolution of the Milky Way Bulge is a very difficult task, but we hope to be able to understand the major events, or establish an approximate sequence for its development, aided by the study of Bulge chemical evolution. We have learned relatively recently how to interpret the chemical composition of different stellar populations as a result of enrichment by different supernovae and asymptotic giant branch stars. The abundances of different elements act for astronomers as ancient bones do for palaeontologists; they can be used to establish a sequence of generations of stars from past times.

Since high resolution spectroscopy of a large number of stars is prohibitive in terms of observing time, in the past the metallicity distribution was determined via low resolution spectra for a few hundred stars and sometimes obtaining high resolution spectra only for a few dozen stars, used as calibrators (McWilliam & Rich, 1994). All agreed that the Galactic Bulge was metal-rich, but there was contradictory evidence regarding the mean, spread and shape of the distribution. The Bulge metallicity is far from that of a simple stellar population like a globular cluster, and therefore a large number of stars needed to be measured to sample the whole metallicity range.

The main obstacles to reliable metallicity determination are: the distance and line of sight depth to the Bulge; large and variable reddening; field crowding; and the composite nature of the stellar population. The large mean distance to the Bulge (8 kpc) makes the stars faint, and the non-negligible depth along the line of sight makes it difficult to determine the absolute stellar luminosities accurately. The large reddening makes stars fainter and redder, and its spatial variation adds a significant uncertainty to the conversion between colour and effective temperature. Field crowding is a real issue, because it is always difficult to determine whether the spectrum we are looking at has been emitted by one star, or represents the superposition of several. The composite nature of the stellar population is due not only to the fact that we have to look throughout the Galactic disc, but also to the possible presence of disc as well as halo stars *in situ*. When measuring chemical compositions, it is difficult to tell if we are looking at a true Bulge star, and we would have to resort to other evidence (such as photometry and kinematics).

Our brave team of astronomers was not daunted by these difficulties, and decided to undertake the major enterprise of measuring elements for Bulge red giants. In this *tour de force* we measured hundreds of Bulge stars, which is a sample size more than an order of magnitude larger than earlier studies. While we have not found all the answers, we are extremely pleased with the progress made using ESO telescopes. This is our story and the major results.

Data for Bulge red giants

Target selection

In the colour-magnitude diagram illustrated in Figure 1, the target stars are located on the red giant branch (RGB), roughly one magnitude above the red clump. The astrometry and the V, I photometry come from OGLE and ESO Wide Field Imager (WFI) observations. Cross-identification with the 2MASS point source catalogue (Carpenter et al., 2001) allowed us to obtain V, I, J, H and K magnitudes for each of the target stars. Some of the fields contain a globular cluster, namely NGC 6528 and NGC 6522 in Baade's Window, NGC 6558 in the $b = -6^{o}$ field, and NGC 6553 in the eponymous field. Member stars of these clusters are the subject of other dedicated papers (see Barbuy et al., 2007, for NGC 6558). Also, in order to avoid strong biases in the resulting iron distribution function (IDF), we included targets spanning the whole colour range of the RGB at that magnitude.

Observations with FLAMES

Spectra for a sample of K giants in four Bulge fields have been collected at the VLT-UT2 with the FLAMES–GIRAFFE spectrograph, at resolution R ≈ 20 000. A total wavelength range of about 760 Å has been covered through the setup combinations HR 13 + HR 14 + HR 15 (programme 071.B-0617), and HR 11 + HR 13 + HR 15 (programme 073.B-0074) for different

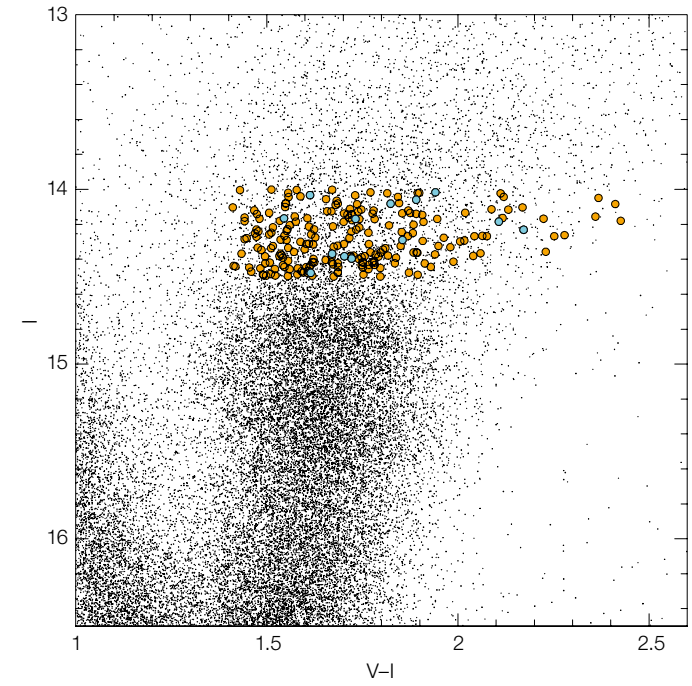

Figure 1. The location of target stars in the colour-magnitude diagram of the field at b = –6°. GIRAFFE targets are marked in orange, UVES ones in cyan. The broad vertical sequence is the Bulge red giant branch, with the red clump just below our targets. Partially visible as a vertical sequence on the left is the disc main sequence, spread along the line of sight.

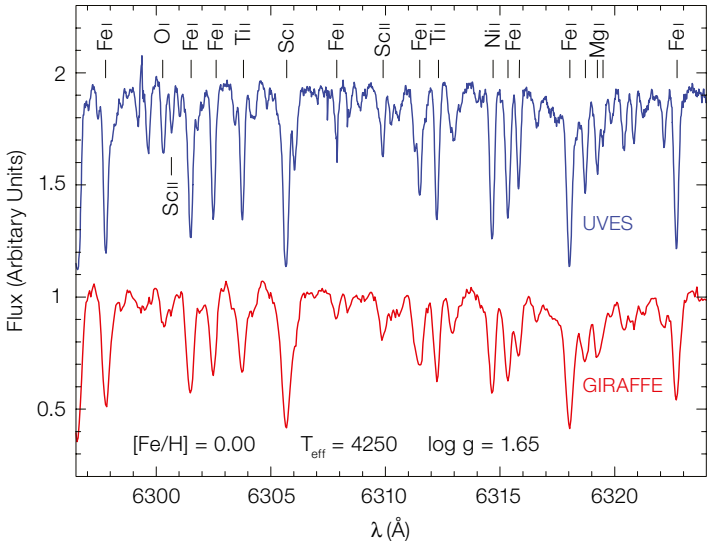

Figure 2. The spectrum of a typical star of our sample, as observed with UVES (top) and GIRAFFE (bottom). The oxygen line at 6300 Å and the magnesium triplet at 6318 Å are marked, together with all the other identified lines. The high density of spectral lines is evident, complicating the location of the stellar continuum.

fields. A portion of a typical star spectrum observed with both the GIRAFE and UVES modes is shown in Figure 2. The characteristics of the observed fields, together with the number of target stars contained in each, are listed in Table 1. The total exposure time varied from about 1 hour to almost 5 hours, depending on the setup and on the star luminosity (targets have been divided into a bright and a faint group) in order to ensure that the final signal-to-noise (S/N) of each co-added spectrum is around 60.

In fact, the actual S/N is not identical among the targets of a given field. Simultaneous to the GIRAFFE observations we collected UVES spectra for around 50 stars, in common with the GIRAFFE sample. These higher resolution spectra (R ~ 45 000) are useful for more precise determinations of element abundances and a check for systematic errors in the GIRAFFE (R ~ 22 000) measurements.

Individual spectra were reduced with the GIRBLDRS pipeline provided by the FLAMES consortium, including bias, flatfield, extraction and wavelength calibration. All the spectra for each star (a number between 1 and 5, depending on the field) were then registered in wavelength to correct for heliocentric radial velocity and co-added to a single spectrum per setup, per star. In each plate, about 20 GIRAFFE fibres were allocated to empty sky regions. These sky spectra were visually inspected to reject the few that might have evident stellar flux, and then co-added to a single sky spectrum. The latter was then subtracted from the spectrum of each target star. The equivalent widths (EWs) for selected iron lines were measured using the automatic code DAOSPEC (Stetson & Pancino, 2008).

Analysis of abundances and errors

The V–I colour was used to obtain photometric temperatures, based on the infrared flux method. As an additional indicator of the star temperature we measured the strength of the TiO band using an index defined between 6190–6250 Å (band) and 6120–6155 Å (continuum region). Finally, it is worth emphasising that the photometric temperature has only been used as an initial first guess. The final adopted temperature is the spectroscopic one, derived imposing excitation equilibrium on a sample of around 60 Fe I lines.

Photometric gravity was calculated from the mass and the radius, the latter derived from the Stefan–Boltzman law, relating the total flux (absolute bolometric magnitude), the temperature and the radius of a blackbody. For this calculation we have adopted a mean distance of 8 kpc for

Nr.	Identification	*l*	*b*	R_{GC} (pc)	*E(B–V)*	N_{stars}
1	Baade's Window	1.14	–4.18	604	0.55	204 (+ 205)
2	b = –6° field	0.21	–6.02	850	0.48	213
3	b = –12° field	0.00	–12.0	1663	0.20	104
4	NGC 6553 field	5.25	–3.02	844	0.70	201

Table 1. Characteristics of the four Bulge fields. In column 5 R_{GC} is the offset distance from the Galactic Centre.

the Bulge, $T_{\odot}$ = 5770 K, log $g_{\odot}$ = 4.44, $M_{\odot,bol}$ = 4.75 and M* = 0.85 $M_{\odot}$. Note that, at each step of the iterative process used to converge on the stellar parameters and metallicity, described below, the photometric gravity was re-calculated using the appropriate (spectroscopic) temperature and metallicity.

Local Thermodynamic Equilibrium (LTE) abundance analysis was performed using standard procedures and the new MARCS spherical models. Excitation equilibrium was imposed on FeI lines in order to refine the photometric T_{eff}, while photometric gravity was imposed, even if ionisation equilibrium was not fulfilled. The microturbulence velocity (V_T) was found by imposing a constant [Fe/H] for lines of different expected strengths (predicted EWs for a given stellar model). Finally, once converged on the best stellar parameters, we calculated the [Fe/H] of each star as a weighted mean of the line-by-line measurements. The weight associated with each line is given by the inverse square of its abundance error, as derived from the error in the measured EWs.

There are three independent estimates of the internal errors: i) via repeated and independent analysis; ii) by comparison with the UVES results; and iii) using globular cluster stars. These indicate $\sigma_{[Fe/H]}$ = 0.09, 0.16, and 0.12 dex, respectively. Figure 3 shows a comparison between GIRAFFE and UVES iron abundances for stars observed with both setups. All those estimates include the smaller (< 0.06 dex) statistical error due to line-to-line dispersion, but each of them includes only a subset of all the possible causes of errors. Putting together the different tests, and considering that some of the systematics (non-LTE effects, uncertainties in the model atmospheres themselves, etc.) have not been taken into account here, we can conclude that ± 0.2 dex is a conservative estimate of our uncertainty on the metallicity of an individual star, including both the effect of statistics and systematics.

Results: the detailed Bulge chemical abundances

The contamination due to disc and halo

Before analysing the abundances, we boldly estimated the contamination in the survey fields coming from the Galactic thin disc, thick disc and halo using an updated version of the Besancon Galaxy model (Robin et al., 2003). Simulated colour-magnitude diagrams (CMDs) have been constructed for the three fields along the Bulge minor axis. Minor adjustments were made in the assumed reddening law to ensure that the simulated red clump would coincide in colour and magnitude with the observed one. The model CMDs reproduce well many characteristics of the observed CMDs, although some differences, especially in the colour spread (likely due to differential reddening), are evident.

Contaminating foreground thin disc stars are estimated to be giant stars (not dwarfs as one might naively expect) located mostly between 2 and 5 kpc from the Sun. The contamination from the halo population turns out to be between zero and 2% in all the fields, and hence it can be safely neglected.

Finally, note that our knowledge of the disc properties far from the Sun is still extremely poor. The Besancon model predicts many thick disc stars in the central region of our Galaxy. However, there is certainly a hole in the HI and CO distribution inside ~3 kpc, and we know that in most barred galaxies disc stars are cleaned up in the central region. We do not know if the real thick disc follows the thin disc and gas distribution, or whether it keeps growing towards the centre. Thus, the relative contributions of the various Galactic components in fields so close to the Galactic Centre need to be handled with caution.

The Bulge metallicity gradient

Based on the metallicity distribution obtained from high dispersion spectroscopy of hundreds of stars in different Bulge fields, we confirm that the Bulge is predominantly metal-rich, with a metallicity dispersion much larger than the errors.

The iron distribution functions (IDFs) obtained in the three fields along the Bulge minor axis are shown in Figure 4. We do not show the IDF for the field around NGC 6553 here as this field has the strongest differential reddening, and none of the reddest stars were included in our target list. In addition, the separation between cluster and field stars is very difficult to establish in this field because the cluster shares the mean

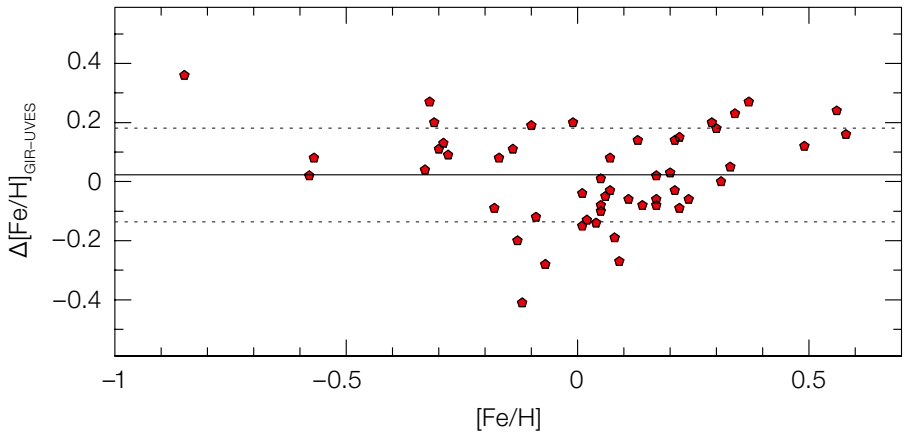

Figure 3. Difference between the [Fe/H] abundance ratio measured in the GIRAFFE and in the UVES spectra for the same stars. The mean difference between the two (solid line) is consistent with zero on average, and, in particular, around [Fe/H] = 0 where most of our stars are located. The spread of the distribution (dotted lines) is σ = 0.16 dex, included in our conservative error estimate of $\sigma_{[Fe/H]}$ = ± 0.2 dex, for the GIRAFFE spectra.

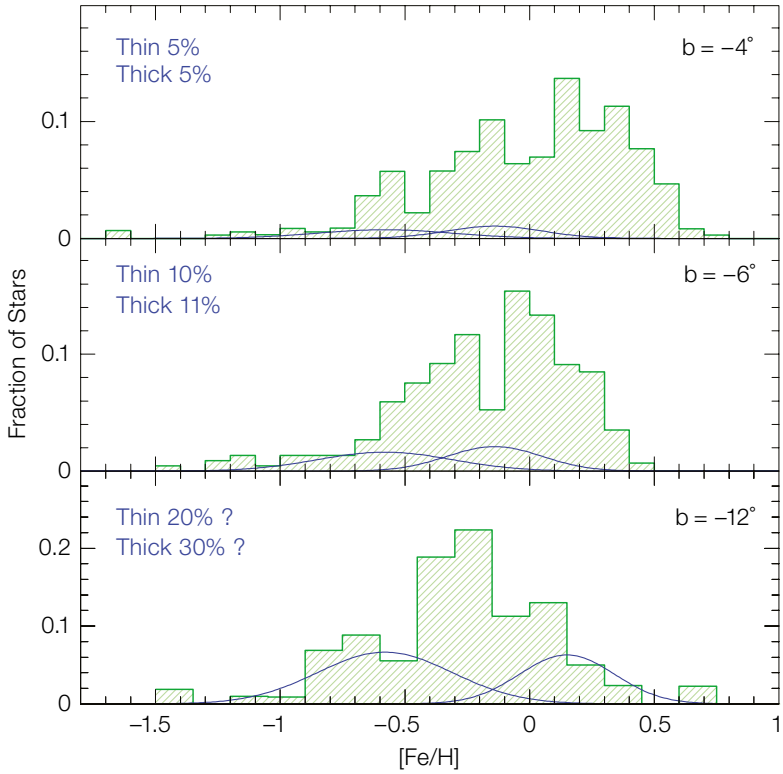

Figure 4. Iron Distribution Function (IDF) in the three fields along the Bulge minor axis. The innermost field (upper), at Galactic latitude b = −4° (Baade's Window) contains 409 target stars, with mean metallicity <[Fe/H]> = +0.03. The intermediate field (middle) at b = −6° includes 213 target stars, with <[Fe/H]> = −0.17. The outermost field (lower) at latitude b = −12°, includes 104 target stars, with <[Fe/H]> = −0.28. The blue Gaussians qualitatively show the percentage of target stars estimated to belong to the Galactic thin and thick disc, and their approximate IDF, assuming it is similar to the thin/thick disc IDF in the Solar Neighbourhood.

metallicity and radial velocity of Bulge stars. Figure 4 clearly shows a difference in the mean metallicity of the three fields, with the inner one being on average more metal-rich than the intermediate and outer one. Two Gaussians are plotted over the metallicity distribution of Bulge stars (histograms) showing the estimated percentage contamination by thick and thin discs. The Gaussians do have the mean and sigma values characteristic of the thick (Reddy et al., 2006) and thin disc (Nordström et al., 2004) IDF, in the Solar Neighbourhood. According to the model, the contaminating disc stars are closer to the Bulge than to us, but the inner disc radial gradient for intermediate-age and old stars has never been measured, hence where exactly these Gaussians would lie is not very well known.

The Baade's Window IDF has been derived from the combination of our data, plus a very similar set of spectra for red clump stars, obtained within the GTO programme and reduced in a consistently way (cf. Lecureur et al., 2009, in preparation). In spite of the uncertainty on the mean metallicity of the contaminating disc stars, it is clear that their number is negligible in this field. The IDF of the field at b = −6° has been derived from 213 giant stars and shows a hint of bimodality, unlike the other fields. Again, the relative disc contamination is low in this field, and would not have a significant impact on the shape of the derived Bulge IDF. The field at b = −12° has the lowest metallicity, but also the highest field contamination (due to a very rapid decrease of the Bulge density with respect to the disc one), thus the highest uncertainty in the true Bulge IDF. However even if we consider only the innermost two fields, there is a radial metallicity gradient, with the IDF mean value going from <[Fe/H]> = +0.03 at b = −4° to <[Fe/H]> = −0.12 at b = −6°. More specifically, it seems that rather than a solid shift towards more metal-poor mean values, it is the metal-rich stars that gradually disappear, while the metal-poor ones are always roughly in the same position.

Metallicity dependence on kinematics

We studied the dependence of the radial velocities versus metallicity for Bulge field stars in the three fields. First, as expected, the velocity dispersion (σ_{RV}) goes down along the Bulge minor axis, from σ_{RV} = 105 km/s in Baade's Window, σ_{RV} = 84 km/s in the b = −6° field, and σ_{RV} = 80 km/s in the field at b = −12°. The latter would be further reduced to σ_{RV} = 60 km/s if the five stars with absolute velocity $|V_{RV}| > 150$ km/s are rejected (e.g., if they are halo stars).

Second, the velocity dispersion of the metal-rich tail is very different in the three fields along the minor axis, being hotter than the metal-poor one in the innermost field, about the same in the intermediate one, and extremely cold in the outermost field. The outermost field is contaminated with disc stars, and we propose that the metal-rich tail is in fact made up of thin disc stars. On the other hand, the two innermost fields have negligible disc contamination, and the interpretation of the different kinematics of the metal-rich component with respect to the metal-poor one is not straightforward (Babusiaux et al., 2009, in preparation).

The important light elements O, Mg, Na and Al in the Bulge

We measured oxygen, magnesium, sodium and aluminum in the 50 K-giants observed through the FLAMES simultaneous fibre link to UVES. These have [Fe/H] covering a wide metallicity range, from −0.8 to + 0.3 (Zoccali et al., 2006; Lecureur et al., 2007). The result is shown in Figure 5, where it is evident that Bulge stars have larger [O/Fe] and [Mg/Fe] than both thin and thick disc stars. This is the signature of a chemical enrichment by massive stars, progenitors of Type 2 Supernovae (SNII), with little or no contribution from SNIa, and thus of a shorter formation timescale of the Bulge with respect to both disc components. In this sense, the Bulge (including its globular

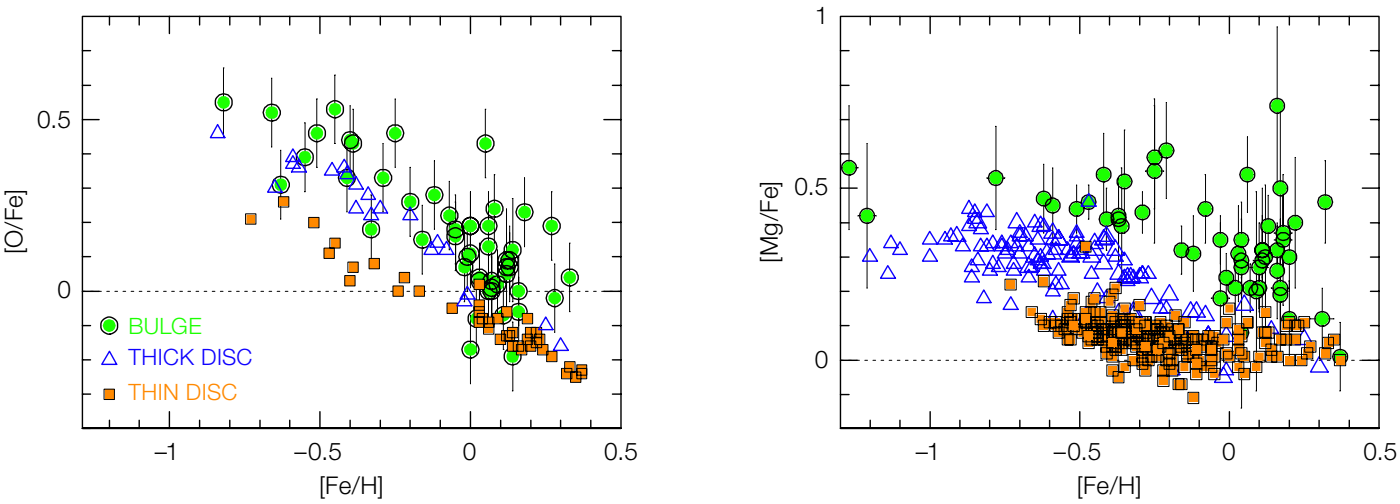

Figure 5. Oxygen to iron (left) and magnesium to iron (right) ratios for Bulge stars, as determined in the present analysis, compared with the same quantities available in the literature for thin and thick disc stars. It is evident that both [O/Fe] and [Mg/Fe] are higher in the Bulge than in the thin and thick disc.

clusters) is the most extreme Galactic population. This result is in agreement with previous studies of a smaller number of stars (10–15) covering a narrower metallicity range (e.g., McWilliam et al., 2003; Rich & Origlia, 2005; Cuhna et al., 2006) and has been confirmed by Fulbright et al. (2007). However, Melendez et al. (2008) found similar [O/Fe] ratios in Bulge and thick disc stars, due to a new abundance analysis of thick disc giants, showing higher oxygen content (while Bulge giants have abundances consistent with the present ones).

Lithium in the Bulge: a scarce element

Lithium, due to its fragility, is expected to be strongly diluted in giants. In marked contrast with this expectation, several Li-rich red giants have been found to date. Very intriguingly, no difference has yet been found between Li-rich stars and those showing normal Li abundance.

The spectra of about 400 K giants, in Baade's Window and the b = –6° fields, including the region around the Li line at 6767.18 Å, were observed. Only 13 of them have a detectable Li line, with six of them having logarithmic abundances A(Li) > 1.5 (González et al., 2009). No clear correlation was found between the Li abundance and those of other elements. Except for the two most Li-rich stars, the others follow a fairly tight A(Li)–T_{eff} correlation. We conclude that there must be a Li production phase during the RGB, acting either on a very short timescale, or selectively only in some stars. The proposed Li production phase associated with the RGB bump cannot be excluded, although our targets are significantly brighter than the predicted RGB bump magnitude for a population at 8 kpc.

What this all means: the formation of the Galactic Bulge

Zoccali et al. (2003) have shown that a simulated CMD with an age of 13 Gyr (which includes the Bulge metallicity distribution) gives a good match to the Bulge CMD. This match includes the luminosity difference between the horizontal branch and the main sequence turnoff, a classical age indicator. However, due to metallicity, reddening, and distance dispersion, the Bulge turnoff cannot be located to better than 0.2–0.3 mag, corresponding to an age uncertainty of ~2–3 Gyr. Conservatively, we take the age of the bulk of Bulge stars to be in excess of 10 Gyr. This limit is confirmed by the recent analysis of a Bulge CMD that was cleaned of foreground disc contamination via proper motions (Clarkson et al., 2008). Such an age limit implies that star formation and chemical enrichment had to be confined within a time interval that is definitely shorter than the age of the Universe at a lookback time of 10 Gyr, or ~3.7 Gyr according to the current concordance cosmology. If the bulk of Bulge stars formed in the cosmic time interval corresponding to a redshift between 3 and 2, then star formation cannot have taken much more than approximately 1 Gyr. Thus, the main uncertainty affecting the duration of the star formation in the Bulge comes from the uncertainty in its age: the older it is, the shorter the star formation era.

The second constraint on the formation timescale of the Bulge comes from the measured alpha-element enhancement (Barbuy et al., 2006; Zoccali et al., 2004, 2006; Lecureur et al., 2007). This is interpreted as a result of the interplay of the fast delivery of iron-poor nucleosynthesis products of massive stars by SNII, with the slow delivery of iron-rich products by SNIa. A star formation timescale of approximately 1 Gyr is generally derived from chemical evolution models, which typically assume a distribution of SNIa delay times. Thus, the derived timescale is modulo the adopted distribution of SNIa delay times. Other equally plausible distributions would have given somewhat shorter or longer timescales. Thus, until the actual mix of SNIa progenitors is fully identified, we shall remain with this uncertainty on how to translate an alpha-element overabundance into a star formation timescale. All in all, combining the

age and the alpha-element enhancement constraints, we conclude that the formation of the Bulge cannot have taken much longer than approximately 1 Gyr.

In addition, the radial metallicity gradient found here would argue against the formation via secular evolution of the bar, because obviously the vertical heating that transforms a bar into a pseudo-bulge would not act preferentially on metal-poor stars. However, combining our result with previous ones on the inner Bulge, at the moment there is evidence of a flat metallicity distribution inside ~600 pc, and a radial gradient outside. Should those findings be confirmed, they might indicate the presence of a double-component Bulge, an inner pseudo-bulge, and an outer classical one, as already found by Peletier et al. (2007) within the SAURON survey of galaxy bulges.

Finally, concerning the Bulge chemical evolution, from the IDF we conclude that the Bulge must have accreted primordial gas, due to the lack of metal-poor stars with respect to the simple model prediction (the so-called G dwarf problem, solved with the inclusion of some infall in the model) and must have ejected a substantial fraction of the iron it produced (outflow). In addition, from the overabundance of alpha-elements quoted above, we can conclude that the Bulge cannot have accreted stars already significantly enriched by SN Ia products, such as disc stars, or stars born in the surviving satellite galaxies in the Local Group.

We are currently completing the analysis by measuring the alpha-elements in the complete GIRAFFE sample. The different abundances of these elements in Bulge and disc stars will allow us to pose a stronger constraint on the fractional disc contamination in the IDFs of Figure 4. In addition, we will measure other heavier elements, adding independent constraints on the chemical enrichment history, thus the formation timescale. We look forward to the E-ELT: its fantastic collecting power, coupled with the high spectral resolution of one of the proposed instruments (the near-IR spectrograph SIMPLE, at R ~ 100 000), will allow us to measure abundances in Bulge main sequence stars. These are hotter, thus have cleaner continua, and are unevolved, i.e., they maintain on their surface the exact chemical pattern of the gas from which they were born.

References

Barbuy, B. et al. 2007, AJ, 134, 1613
Bensby, T., Feltzing, S. & Lundström, I. 2004, A&A, 421, 155
Clarkson, W. 2008, ApJ, 684, 1110
Cuhna, K. & Smith, V.V. 2006, ApJ, 651, 491
Fulbright, J.P., McWilliam, A. & Rich, R.M. 2007, ApJ, 661, 1152
González, O. et al. 2009, A&A, submitted
Lecureur, A. et al. 2007, A&A, 465, 799
McWilliam, A. & Rich, R.M. 1994, ApJ, 91, 749
McWilliam, A. & Rich, R.M. 2003, in *Origin and Evolution of the Elements*
Melendez, J. et al. 2008, A&A, 484, L21
Nordström, B. et al. 2004, A&A, 418, 989
Peletier, R. et al. 2007, MNRAS, 379, 445
Reddy, B.E., Lambert, D.L. & Allende Prieto, C. 2006, MNRAS, 367, 1329
Rich, R.M. & Origlia, L. 2005, ApJ, 634, 1293
Stetson, P., & Pancino, E. 2008, PASP, 120, 1332
Zoccali, M. et al. 2003, A&A, 399, 931
Zoccali, M. et al. 2006, A&A, 457, L1
Zoccali, M. et al. 2008, A&A, 486, 177

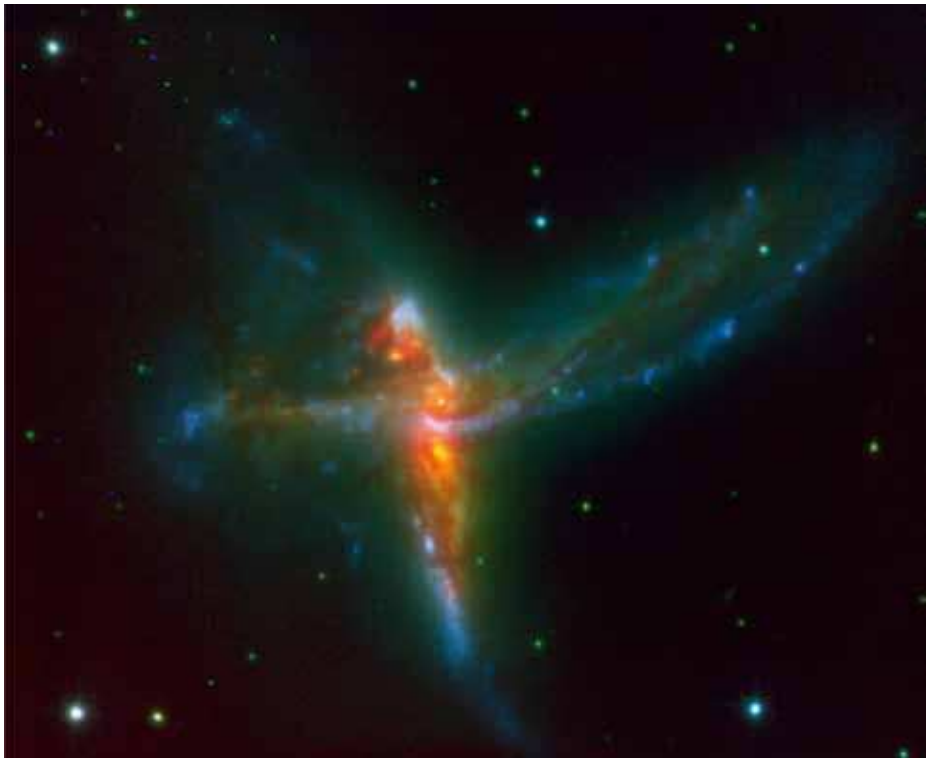

A VLT/NACO *K*-band exposure was combined with HST/ACS B and *I*-band images to form this colour image of the interacting galaxy system ESO 593-IG 008 (IRAS 19115-2124), dubbed "The Cosmic Bird". The three components are a barred spiral, an irregular galaxy and an irregular luminous infrared galaxy (the head of the Bird) with a very high rate of star formation (~ 200$M_{\odot}$/year). See ESO PR 39/08 for details.